Theory of enhancement of thermoelectric properties of materials with nanoinclusions

Sergey V. Faleev and François Léonard*
Sandia National Laboratories, Livermore, California 94551, USA
(Received 19 March 2008; published 12 June 2008)

Based on the concept of band bending at metal/semiconductor interfaces as an energy filter for electrons, we present a theory for the enhancement of the thermoelectric properties of semiconductor materials with metallic nanoinclusions. We show that the Seebeck coefficient can be significantly increased due to a strongly energy-dependent electronic scattering time. By including phonon scattering, we find that the enhancement of *ZT* due to electron scattering is important for high doping, while at low doping it is primarily due to a decrease in the phonon thermal conductivity.

DOI: 10.1103/PhysRevB.77.214304 PACS number(s): 73.63.−b, 65.40.−b, 72.10.−d, 72.15.Eb

I. INTRODUCTION

The energy conversion efficiency of thermoelectric devices depends on the figure of merit $ZT=S^2\sigma T/\kappa$, where S, σ, T, and κ are the Seebeck coefficient, electrical conductivity, temperature, and thermal conductivity. In the best thermoelectric materials ZT is typically ~ 1, and it is difficult to increase ZT beyond this value because of competing effects of electrical and thermal conductivities. Advances over the past decade show that it is possible to enhance ZT in nanostructured thin-film systems by taking advantage of quantum confinement to enhance the power factor $S^2\sigma$,[1] or to increase phonon scattering at interfaces to reduce the lattice contribution to κ.[2] On the other hand, many existing and envisioned thermoelectric applications will require a material that is itself of macroscopic dimension. Therefore, recent reports of property enhancement in bulk alloys possessing nanometer-scale compositional modulations have generated much excitement.[3–6] ZT values as high as 2.2 have been reported[3,4] in the $(PbTe)_x(AgSbTe_2)_{1-x}$ system and have been ascribed to a large Seebeck coefficient and low lattice thermal conductivity due to nanoscale clustering of Ag and Sb. Heremans *et al.*[5] reported that the Seebeck coefficient in bulk PbTe can be increased significantly by precipitating a fine distribution of Pb nanoinclusions, and suggested heuristically that the increase in Seebeck coefficient originates from an energy-filtering effect due to a strongly energy-dependent electronic scattering time. Kim *et al.*[6] observed an enhancement of the thermoelectric properties when ErAs nanoparticles of 2.4 nm average diameter were embedded in a InGaAs matrix, and ascribed the increase to a reduction in the phonon thermal conductivity. Given these observations, a general understanding of the role of nanoinclusions in enhancing the thermoelectric properties of materials is needed, in particular to assess the relative importance of electronic and phonon scattering.

In this paper we present a theoretical model and numerical calculations of the thermoelectric properties of bulk semiconductors containing metallic nanoparticles. Our model considers scattering of electrons on the band bending at the interfaces between the semiconductor host and randomly distributed metallic islands. This causes energy-dependent scattering of electrons, leading to an energy filtering effect that increases the Seebeck coefficient. This provides an explicit physical model for the proposed energy filtering effect.[5] By combining this model with a model for phonon scattering on the nanoinclusions, we predict significant enhancement of the ZT factor.

We point out that while the role of metallic nanoinclusions may appear at first to be similar to that of point defects for which extensive work has been done, the physics is actually quite different. Indeed, in addition to the electronic scattering, the phonon scattering on nanoinclusions occurs in a completely different regime than that on point defects, as will be discussed in Sec. IV B.

The central idea in this paper is illustrated in Fig. 1. There, spherical metallic nanoinclusions with radius R and volume fraction x are randomly distributed in a bulk semiconductor material. In general, at such metal/semiconductor interfaces, charge transfer between the metal and the semiconductor leads to band bending away from the interface,

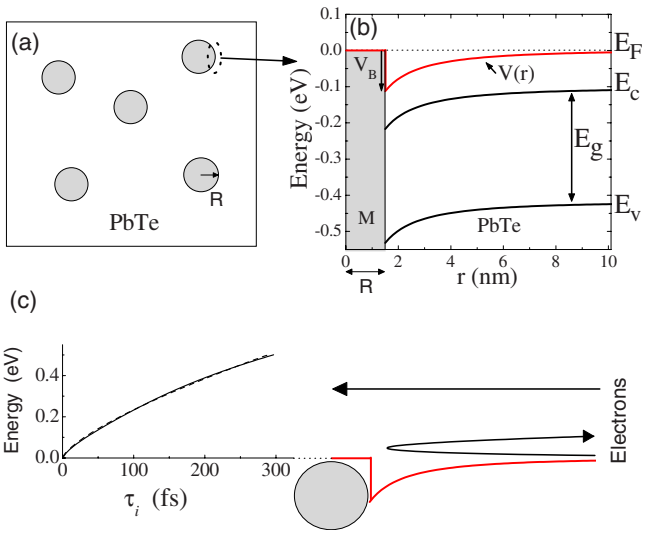

FIG. 1. (Color online) (a) Schematic of the semiconductor host with metallic nanoinclusions. Panel (b) shows an example of the calculated potential $V(r)$ and the energy diagram for PbTe at $T=300$ K, $n=2.5\times10^{19}$ cm^{-3}, $V_B=-0.11$ eV, and $R=1.5$ nm. Panel (c) illustrates the concept of energy filtering: low energy electrons scatter strongly with the potential, but high energy electrons are unaffected. The calculated electronic relaxation time for the potential of panel (b) is also shown.

characterized by the electrostatic potential $V(r)$ [Fig. 1(b)]. The presence of this potential causes *energy-dependent* scattering of electrons, as illustrated in Fig. 1(c). The high-energy electrons are unaffected by the potential, but the low energy electrons can be strongly scattered. Because the Seebeck coefficient depends on the energy derivative of the relaxation time $d \ln \tau(E)/dE$ at the Fermi energy, this type of energy filtering is precisely the prescription to increase the Seebeck coefficient of thermoelectric materials.

Our theoretical model is based on the Boltzmann transport equation (BTE) within the relaxation time approximation. We apply the model to a system of n-doped PbTe with metallic nanoinclusions because of the availability of experimental data and good understanding of scattering mechanisms in bulk PbTe,[7–9] although the theory can be used for any thermoelectric material.

II. CHARGE AND HEAT TRANSPORT IN BULK PbTe

In this section we will review the expressions[7–9] for the charge and heat transport in bulk PbTe with n-type doping. The valence band of PbTe contains four energy minima located at the L points. The energy dispersion relation near each minimum is usually described by the Kane model[8]

$$\frac{\hbar^2 k_l^2}{2m_l^*} + \frac{\hbar^2 k_t^2}{m_t^*} = E(1 + E/E_g), \tag{1}$$

where E_g is the direct energy gap of PbTe, $\hbar$ is the Planck constant, and k and m^* are the electron wave vector and effective mass (at minimum energy point $k=0$, $E=0$) along the longitudinal (suffix l) and transverse (suffix t) directions of the corresponding L point. For n-type PbTe the electron concentration is given by

$$n[E_F] = \frac{(2m_d^* k_B T)^{3/2}}{3\pi^2\hbar^3} \int_0^\infty \gamma(z)^{3/2} \left(-\frac{\partial f_0}{\partial z}\right) dz, \tag{2}$$

where $m_d^* = 4^{2/3}(m_l^* m_t^{*2})^{1/3}$ is the density of states effective mass in which the fourfold degeneracy is included, k_B is the Boltzmann constant, and $f_0(z)$ is the Fermi function written in terms of dimensionless variables $z = E/(k_B T)$ and $z_F = E_F/(k_B T)$. E_F is the Fermi energy and the function $\gamma(z) = z + bz^2$, where $b = k_B T/E_g$. In the relaxation time approximation the BTE expressions for electrical conductivity, σ, Seebeck coefficient, S, and electron contribution to thermal conductivity, κ_e, are[8]

$$\sigma = \frac{e^2}{m_c^*} \frac{(2m_d^* k_B T)^{3/2}}{3\pi^2\hbar^3} \langle \tau(z) \rangle, \tag{3}$$

$$S = \frac{k_B}{e} \frac{\langle \tau(z)(z - z_F) \rangle}{\langle \tau(z) \rangle}, \tag{4}$$

and

$$\kappa_e = \sigma T \frac{k_B^2}{e^2} \left\{ \frac{\langle \tau(z) z^2 \rangle}{\langle \tau(z) \rangle} - \left[\frac{\langle \tau(z) z \rangle}{\langle \tau(z) \rangle} \right]^2 \right\}, \tag{5}$$

where $m_c^* = 3/(1/m_l^* + 2/m_t^*)$ is the effective conductivity mass, and the average is defined as

$$\langle A(z) \rangle \equiv \int_0^\infty \frac{\gamma(z)^{3/2}}{1 + 2bz} \left(-\frac{\partial f_0}{\partial z}\right) A(z) dz. \tag{6}$$

In bulk PbTe at room temperature the dominant contributions to the total relaxation time, $\tau_{\text{bulk}}(z)$, are scattering by the deformation potential of acoustic and optical phonons, and polar scattering by optical phonons.[7–9] We also take into account scattering on the short-range potential of vacancies although it gives a much smaller contribution compared to scattering by phonons. Thus, the total relaxation time for bulk PbTe is given by

$$\frac{1}{\tau_{\text{bulk}}(z)} = \frac{1}{\tau_{\text{PO}}(z)} + \frac{1}{\tau_a(z)} + \frac{1}{\tau_o(z)} + \frac{1}{\tau_v(z)}. \tag{7}$$

The relaxation time due to polar scattering by optical phonons reads[8,9]

$$\tau_{\text{PO}}(z) = \frac{\hbar^2 \gamma(z)^{1/2} F^{-1}}{e^2 (2m_{d1}^* k_B T)^{1/2} (\epsilon_\infty^{-1} - \epsilon_0^{-1}) \gamma'(z)}, \tag{8}$$

where $m_{d1}^* = (m_l^* m_t^{*2})^{1/3}$ is the density of states effective mass in the single valley, the function $\gamma'(z) = 1 + 2bz$, ϵ_0 and ϵ_∞ are the static and high frequency permittivities, and

$$F = 1 - \delta \ln\left(1 + \frac{1}{\delta}\right) - \frac{2bz(1 + bz)}{(1 + 2bz)^2} \times \left[1 - 2\delta + 2\delta^2 \ln\left(1 + \frac{1}{\delta}\right)\right]. \tag{9}$$

Here $\delta = (2kr_0)^{-2}$ with r_0 the screening length of optical phonons:

$$r_0^{-2} = \frac{2^{5/2} e^2 m_d^{*3/2} (k_B T)^{1/2}}{3\pi^2\hbar^3} \int_0^\infty \gamma(z)^{1/2} \gamma'(z) \left(-\frac{\partial f_0}{\partial z}\right) dz. \tag{10}$$

The relaxation time due to scattering by the deformation potential of acoustic and optical phonons, and also due to scattering on the short range potential of vacancies can be written generally as[8,9]

$$\tau_m(z) = \frac{\tau_{0,m}}{\gamma(z)^{1/2} \gamma'(z) [(1 - A)^2 - B]}, \tag{11}$$

where $A = bz(1 - K_m)/\gamma'(z)$, and $B = 8bz(1 + bz)K_m/(3\gamma'^2(z))$, with the suffix $m = a$ for acoustic phonons, $m = o$ for optical phonons, and $m = v$ for vacancies. The constants $\tau_{0,m}$ and K_m are defined as

$$\tau_{0,a} = \frac{2\pi\hbar^4 C_l}{E_{ac}^2 (2m_{d1}^* k_B T)^{3/2}}, \quad K_a = \frac{E_{av}}{E_{ac}}, \tag{12}$$

$$\tau_{0,o} = \frac{2\hbar^2 a^2 (\hbar\omega_0)^2 \rho}{\pi E_{oc}^2 (2m_{d1}^* k_B T)^{3/2}}, \quad K_o = \frac{E_{ov}}{E_{oc}}, \tag{13}$$

and

TABLE I. Parameters used to calculate the relaxation times for bulk PbTe at $T=300$ K.[9] m_0 is the free electron mass.

Parameter	Value	Parameter	Value
E_g	0.315 eV	$\hbar\omega_0$	0.0136 eV
m_t^*/m_0	0.0453	a	6.461 Å
m_l^*/m_0	0.24	ρ	8.24 g/cm
ϵ_0	400	E_{ac}	15 eV
ϵ_∞	32.6	E_{oc}	26 eV
C_l	7.1×10^{10} N/m	$K_{a,o}$	1.5
U_{vc}	3×10^{-34} erg cm^3	K_v	1.5

$$\tau_{0,v}=\frac{\pi\hbar^4}{U_{vc}^2 m_{d1}^*(2m_{d1}^* k_B T)^{1/2}N_v},\quad K_v=\frac{U_{vv}}{U_{vc}}. \tag{14}$$

Here C_l is a combination of elastic constants, E_{ac} and E_{av} are the acoustic phonon deformation potential coupling constants for conduction and valence bands, E_{oc} and E_{ov} are optical phonon deformation potential coupling constants for conduction and valence bands, U_{vc} and U_{vv} are coupling constants of the short range potential of vacancies for conduction and valence bands, a is the lattice constant, ω_0 is the frequency of optical phonons, and ρ is the mass density. N_v is the concentration of vacancies calculated from the condition that one vacancy gives two charge carriers, $N_v=n/2$.

The parameters used for calculation of the relaxation times in bulk PbTe at $T=300$ K are taken from Ref. 9. These parameters are shown in Table I. For calculations at different temperatures we assumed the values of these parameters to be the same as for $T=300$ K except for E_g and m_t^*, which were linearly interpolated and extrapolated using $T=4.6$ K and $T=300$ K values,[9] with E_g saturating for $T>400$ K.[8]

III. ELECTRON SCATTERING ON BAND-BENDING POTENTIAL OF NANOINCLUSIONS

A. Band-bending potential

In our model we assume that spherical metallic nanoinclusions with radius R and volume fraction x are randomly distributed in a n-doped PbTe host material. In this section we will calculate the contribution to the relaxation time due to scattering of electrons on the band-bending potential at the metal-semiconductor interface.

For a *single* nanoinclusion, the electrostatic potential $V(r)$ can be calculated by solving the Poisson equation

$$\frac{\epsilon_0}{4\pi e^2}\frac{1}{r}\frac{d^2}{dr^2}rV(r)=n[E_F]-n[E_F-V(r)]. \tag{15}$$

The right-hand-side of this expression is simply the spatially varying charge [see Eq. (2)] calculated by assuming a rigid shift of the electronic bands with the local potential $V(r)$. We solve the Poisson equation with the boundary conditions $V(\infty)=0$ and $V(R)=V_B$. (V_B is the potential at the semiconductor/metal interface. The value of V_B is fixed for a particular metal and depends on the detailed properties of the interface. However, one may consider it to be an optimization parameter provided that the physics of the metal/semiconductor interface allows tailoring of V_B by choosing the metal.) We used the fourth-order Runge-Kutta and shooting methods in order to solve Eq. (15). Figure 1(b) shows an example of the calculated potential $V(r)$.

For small values of V_B or for large r (when the potential is screened and small) the right-hand-side of Eq. (15) can be linearized with respect to small V:

$$\frac{d^2}{dr^2}rV(r)=\frac{1}{\lambda^2}rV(r), \tag{16}$$

where λ is the screening length. The solution of Eq. (16) is

$$V(r)\propto\frac{1}{r}e^{-r/\lambda}. \tag{17}$$

For degenerate electrons the expression for λ takes the simple form

$$\frac{1}{\lambda^2}=\frac{2e^2(2m_d^*)^{3/2}}{\epsilon_0\pi\hbar^3}\left(E_F+\frac{E_F^2}{E_g}\right)^{1/2}\left(1+2\frac{E_F}{E_g}\right). \tag{18}$$

Due to the large value of the dielectric constant in PbTe, $\epsilon_0=400$, the screening length for typical doping concentrations is several times larger than the wavelength of electrons on the Fermi surface. For example, for $n=5\times10^{19}$ cm^{-3} one can obtain from Eq. (18) $\lambda=11$ nm and $k_F\lambda=7$, where k_F is the wave vector of the electron on the Fermi surface. This value of $k_F\lambda$ slowly varies with doping (for degenerate electrons we can use Eqs. (2) and (18) to obtain the dependence on doping $k_F\lambda\propto n^{1/6}$). On the other hand, a large value of λ can lead to an overlap of the band bending between nanoparticles, which may change the bulk carrier concentration. We have restricted our calculations to a parameter range (doping and inclusion volume fraction) where such effects are not significant.

B. Relaxation time for scattering on nanoinclusions

When the electron scattering on nanoinclusions is taken into account, the total relaxation time τ is

$$\tau^{-1}=\tau_{\text{bulk}}^{-1}+\tau_i^{-1}, \tag{19}$$

where the relaxation time for bulk PbTe is given by Eq. (7) and τ_i is the relaxation time due to scattering by $V(r)$ at randomly distributed metallic inclusions

$$\tau_i^{-1}=n_i v\sigma_t. \tag{20}$$

Here

$$n_i=3x/(4\pi R^3) \tag{21}$$

is the concentration of inclusions, σ_t is the electronic transport scattering cross section, and $v=\partial_p E_p$ is the electronic velocity with p the momentum.

In order to calculate the transport cross section in a system with nonparabolic energy dispersion, we consider an electron with momentum $\mathbf{p}$ and wave function $\psi_{\mathbf{p}}(\mathbf{r})=u_{\mathbf{p}}(\mathbf{r})e^{i\mathbf{p}\mathbf{r}/\hbar}$ in the periodic field of the unperturbed PbTe crystal of unit volume. Here $u_{\mathbf{p}}(\mathbf{r})$ is the periodic Bloch am-

plitude. As mentioned earlier, the nonparabolicity of the electron energy dispersion near the conduction band minima is usually described by the Kane model[8]

$$E_p(1+E_p/E_g)=p^2/2m_{d1}^*. \tag{22}$$

The isotropic energy dispersion in a form of Eq. (22) with density of state mass m_{d1}^* is usually assumed in the calculation of the relaxation time.[7–9] The transition probability for scattering from state $\psi_{\mathbf{p}_i}$ to state $\psi_{\mathbf{p}_f}$ per unit time due to a perturbation potential $V(r)$ is given by the standard formula of perturbation theory[10]

$$dw_{fi}=\frac{2\pi}{\hbar}\left|V_{\mathbf{p}_f\mathbf{p}_i}+\int\frac{V_{\mathbf{p}_f\mathbf{p}_1}V_{\mathbf{p}_1\mathbf{p}_i}}{E_{p_i}-E_{p_1}}d\nu_1+\ldots\right|^2 \times\delta(E_{p_f}-E_{p_i})d\nu_f, \tag{23}$$

where $d\nu=d^3\mathbf{p}/(2\pi\hbar)^3$. The matrix elements are

$$V_{\mathbf{p}'\mathbf{p}}\equiv\int\psi_{\mathbf{p}'}^*(\mathbf{r})V(\mathbf{r})\psi_{\mathbf{p}}(\mathbf{r})d^3\mathbf{r}\approx\int e^{i(\mathbf{p}-\mathbf{p}')\mathbf{r}/\hbar}V(\mathbf{r})d^3\mathbf{r}, \tag{24}$$

where we used the fact that collisions with a small momentum transfer dominate scattering on the slow-varying bend-bending potential, therefore, the Bloch amplitudes entering Eq. (24) are rather close to each other, and the overlap factor is about unity $\int u_{\mathbf{p}'}^*(\mathbf{r})u_{\mathbf{p}}(\mathbf{r})d^3\mathbf{r}\approx 1$.

Applying Eq. (24) to Eq. (23), the calculation of dw_{fi} becomes identical to the calculation of the transition probability for scattering of a plane wave $e^{i\mathbf{p}_i\mathbf{r}/\hbar}$ in a model system described by an equation

$$(E_{\hat{p}}+V)\psi=E_p\psi \tag{25}$$

with unperturbed Hamiltonian $E_{\hat{p}}$, $\hat{\mathbf{p}}\equiv-i\hbar\partial_{\mathbf{r}}$, and perturbation potential $V(\mathbf{r})$. Applying the operator $1+E_{\hat{p}}/E_g$ to Eq. (25) one obtains

$$\frac{\hat{p}^2}{2m_{d1}^*}\psi=\left[\frac{p^2}{2m_{d1}^*}+\frac{V^2}{E_g}-V\left(1+2\frac{E_p}{E_g}\right)\right]\psi. \tag{26}$$

Here we neglect the commutator term $E_g^{-1}[E_{\hat{p}},V(r)]\psi$

$$E_g^{-1}[E_{\hat{p}},V(r)]\approx\frac{E_F}{E_g}\frac{1}{(k_F\lambda)^2}V(r)\ll V(r) \tag{27}$$

using the fact that $rV(r)$ is a slow varying function and $k_F\lambda\gg 1$.

Equation (26) has the form of the usual Schrödinger equation that can be used for numerical solution of the scattering problem with a potential

$$U_p(r)=V(r)\left(1+2\frac{E_p}{E_g}\right)-\frac{V^2(r)}{E_g}. \tag{28}$$

C. Calculation of transport cross section

The transport cross section for scattering on the spherically symmetric potential is given by[10]

$$\sigma_t=2\pi\int_0^\pi|f(\theta)|^2(1-\cos\theta)\sin\theta d\theta, \tag{29}$$

where $f(\theta)$ is the scattering amplitude defined from the large -r asymptote of the wave function

$$\psi\approx e^{i\mathbf{p}\mathbf{r}/\hbar}+\frac{f(\theta)}{r}e^{ipr/\hbar}. \tag{30}$$

The wave function ψ is a solution of the Schrödinger Eq. (26) with potential $U_p(r)$ given by Eq. (28). It can be expressed as a sum of contributions with different angular momentum l [10]

$$\psi=\sum_{l=0}^{\infty}P_l(\cos\theta)R_{kl}(r), \tag{31}$$

where P_l are the Legendre polynomials and $R_{kl}(r)$ are solutions of the radial Schrödinger equation ($k=p/\hbar$):

$$\frac{1}{r^2}\partial_r r^2\partial_r R_{kl}+\left(k^2-\frac{l(l+1)}{r^2}-\frac{2m_{d1}^*}{\hbar^2}U_p(r)\right)R_{kl}=0. \tag{32}$$

The large-r asymptote of $R_{kl}(r)$ has the form

$$R_{kl}(r)\propto\sin(kr-l\pi/2+\delta_l)/r, \tag{33}$$

where δ_l is the phase shift of $R_{kl}(r)$ relative to the potential-free solution. The scattering amplitude $f(\theta)$ can be expressed in terms of the phase shifts as[10]

$$f(\theta)=\frac{1}{2ik}\sum_{l=0}^{\infty}(2l+1)P_l(\cos\theta)(e^{2i\delta_l}-1). \tag{34}$$

The calculation of the transport cross section (29) with scattering amplitude (34) can be performed in the same way[10] as the usual cross section [without the $(1-\cos\theta)$ factor in Eq. (29)]. In the integrals $\int_0^\pi P_l(\cos\theta)P_{l'}(\cos\theta)(1-\cos\theta)\sin\theta d\theta$ that appear in the evaluation of the transport cross section (29), only terms with $l'=l,l\pm1$ give nonvanishing contributions.[10] After integration over θ, Eq. (29) can be expressed in terms of the δ_l as

$$\sigma_t=\frac{4\pi}{k^2}\sum_{l=1}^{\infty}l\sin^2(\delta_l-\delta_{l-1}). \tag{35}$$

We used the following numerical procedure to solve the Schrödinger equation (32) and calculate the phase shifts. The spherical Bessel function $j_l(kr)$ is a regular solution of Eq. (32) for $r<R$, in the region where $U_p(r)=0$. We used the fourth-order Runge-Kutta method to solve Eq. (32) for $r>R$ with boundary conditions such that the solution $R_l(kr)$ and its derivative match the spherical Bessel function at $r=R$. At some large $r=r_{\max}$ we assume that the potential U_p vanishes and match the solution $R_l(kr)$ and its derivative $R_l'(kr)$ to a linear combination of the spherical Bessel function $j_l(kr)$ and spherical Neumann function $y_l(kr)$ (which is another solution of Eq. (32) for $U_p(r)=0$):

$$R_l(kr)|_{r=r_{\max}}\to\alpha j_l(kr)+\beta y_l(kr), \tag{36}$$

with $\alpha=(R_l y_l'-R_l' y_l)/(j_l y_l'-j_l' y_l)$ and $\beta=-(R_l j_l'-R_l' j_l)/(j_l y_l'-j_l' y_l)$. Finally the phase shift δ_l is given by

$$\delta_l = -\arctan(\beta/\alpha). \tag{37}$$

In conjunction with Eqs. (20) and (35) this provide expressions to numerically calculate τ_i for a given $V(r)$. An example of the numerically calculated τ_i is given in Fig. 1(c) for scattering by $V(r)$ of Fig. 1(b), with an inclusion volume fraction $x=5\%$. A simple fit gives the dependence $\tau_i(E) \sim E^{1.39}$ as shown by the dashed line in Fig. 1(c). This energy dependence of τ_i is much stronger than that of τ_{bulk} and leads to enhancement of the Seebeck coefficient.

To obtain an analytical description of $\tau_i(E)$, we also calculated τ_i in the Born approximation by using Fermi's golden rule [first term in r.h.s. of Eq. (23)]

$$\frac{1}{\tau_i^{\text{Born}}} = \frac{p^2}{2\pi\hbar^4}\frac{dp}{dE}\int_0^\pi |V_{\mathbf{p}'\mathbf{p}}|^2(1-\cos\theta)\sin\theta d\theta. \tag{38}$$

Here θ is the angle between initial and final momenta $\mathbf{p}$ and $\mathbf{p}'$. The expression for τ_i^{Born} can be simplified by taking the angle integration in Eq. (38) for $V_{\mathbf{p}'\mathbf{p}}$ and making the substitutions of integration variables $t=2kR\sin\frac{\theta}{2}$ and $y=r/R$. Finally one obtains

$$\tau_i^{\text{Born}}(E) = E^{3/2}\frac{(1+E/E_g)^{3/2}}{1+2E/E_g}\frac{R}{x}\frac{4\sqrt{2m_{d1}^*}}{3\alpha(E,R)}, \tag{39}$$

where

$$\alpha(E,R) = \int_0^{2kR}\left|\int_1^\infty \sin(yt)V(yR)ydy\right|^2 tdt. \tag{40}$$

Numerical tests show that for $|V_B| \lesssim 0.1$ eV, the Born approximation is valid, $\tau_i(E) \approx \tau_i^{\text{Born}}(E)$, while for $|V_B| > 0.1$ eV, $\tau_i^{\text{Born}}(E)$ begins to deviate from $\tau_i(E)$ calculated from the exact solution of Schrödinger's equation (32). Nevertheless, Eq. (39) allows us to analyze the energy dependence of the relaxation time that is difficult to do by using the exact formulas (20) and (35). For energies $E \gtrsim 0.1$ eV, the integral over variable t in (40) weakly depends on the upper limit of the integration, and the function $\alpha(E,R)$ varies slowly with both E and R. Thus, we have $\tau_i^{\text{Born}}(E) \sim E^{3/2}$, in good agreement with the full numerical calculations, which yielded a dependence $E^{1.39}$. Comparing the result $\tau_i^{\text{Born}}(E) \sim E^{3/2}$ with expression (20) (and using $v(E) \sim \sqrt{E}$), we find that the electronic scattering cross section of the band-bending potential depends on energy as E^{-2}; this strong energy dependence is responsible for the superlinear energy dependence of $\tau_i(E)$.

IV. RESULTS AND DISCUSSION

A. Enhancement of the Seebeck coefficient and power factor

The calculation of the total relaxation time allows us to obtain S, σ, and κ_e using expressions (3)–(5). We first consider a specific case by adopting a simple model for the interface potential $V_B=\Phi_m-\chi+E_F$ with Φ_m the metal work function and χ the electron affinity, and choose $\Phi_m-\chi=-0.35$ eV corresponding to Pb nanoinclusions [work function $\Phi_m=4.25$ eV (Ref. 11)] and an electron affinity for PbTe $\chi_{\text{PbTe}}=4.6$ eV.[12] Figure 2 shows the calculated room temperature Seebeck coefficient as a function of the doping n and fixed nanoinclusion volume fraction $x=5\%$. We note the excellent agreement between the experimentally measured S (filled circles)[13] and that calculated numerically (solid line) for bulk PbTe. In addition, one can see that for any nanoinclusion radius, the Seebeck coefficient is always increased compared to that of the inclusion-free system. In fact, for the smallest nanoinclusion radius considered here (1.5 nm), the enhancement in S is over 100% at high doping.

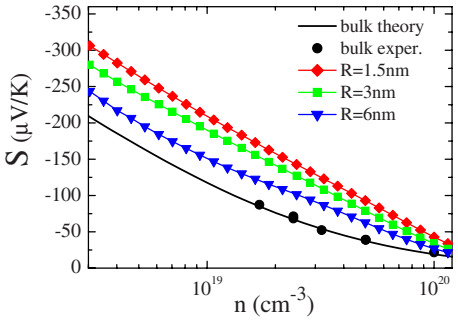

FIG. 2. (Color online) Calculated Seebeck coefficient for PbTe with metallic nanoinclusions as a function of the doping for several different values of the nanoinclusion radius.

It is interesting to consider the impact of V_B on the calculated Seebeck coefficient. Figure 3(a) shows S as a function of V_B. It is clearly seen from this figure that the presence of an extended electrostatic potential leads to an increase in S regardless of the sign of V_B. ($V_B=0$ is equivalent to bulk PbTe with nanoinclusions. Negative values correspond to the situation of Fig. 1, and positive values represent a Schottky barrier). This general behavior can be understood (at least for small $|V_B|$) from the Born approximation, which predicts that the inverse scattering time is proportional to the square of the perturbation potential. With increase of $|V_B|$ the contribution to the total inverse relaxation time from inclusion scattering increases, leading to an increase of S because the energy dependence of τ changes from that of τ_{bulk} to the more strongly energy dependent τ_i. For large values of $|V_B|$ the contribution of island scattering becomes dominant, and S saturates as seen in Fig. 3(a).

Figure 3(a) also shows the calculated values of σ as a function of the interface potential V_B. The conductivity de-

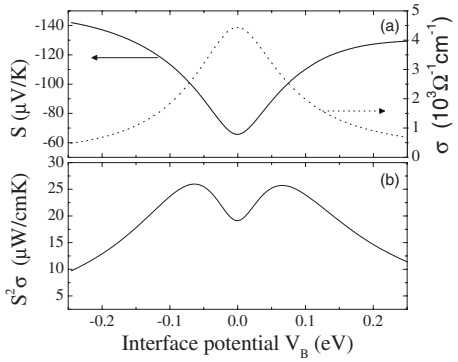

FIG. 3. Panel (a) shows the calculated Seebeck coefficient and conductivity for PbTe as a function of the interface potential V_B. Panel (b) shows the resulting power factor. Parameters are $R=1.5$ nm, $T=300$ K, $x=5\%$, and $n=2.5\times10^{19}$ cm^{-3}.

creases as $|V_B|$ is increased, with a fairly symmetric behavior for $\pm V_B$. Combining the results for σ and S, we obtain the power factor $S^2\sigma$ as depicted in Fig. 3(b). There, one can see that the power factor is increased compared to that at $V_B=0$, in a range of interface potentials $-0.15\ \text{eV} < V_B < 0.15\ \text{eV}$. The power factor has two maxima at some optimal values of V_B because the Seebeck coefficient saturates for large $|V_B|$, while the electrical conductivity σ continues to decrease with increase of $|V_B|$.

For the optimal interface potential $V_B \approx \pm 0.07$ eV, we find that the power factor is increased by $\sim 35\%$. Importantly, the power factor does not decrease substantially over a wide range of values of the interface potential. Thus, it is possible to take full advantage of the reduction in thermal conductivity due to phonon scattering at the nanoinclusions, as we will discuss later.

Instead of optimizing the value of the interface potential V_B to achieve the maximum power factor as shown in Fig. 3(b), we can keep V_B fixed (by choosing a specific metal for the inclusions) and optimize other parameters, for example the inclusion volume fraction or radius. To analyze the dependence of the transport coefficients on these parameters, we can use Eq. (39). As we noted above, the function $\alpha(E,R)$ in Eq. (40) varies slowly with both E and R, so the inverse relaxation time due to electron scattering by inclusions can be approximated as $\tau_i^{-1}(E) \approx CE^{-3/2}$, where the constant C depends on V_B, x, and R mostly through the combination (at least for small V_B)

$$C \propto V_B^2 x/R. \tag{41}$$

In turn, the transport coefficients (S, σ, and κ_e) depend only on this ratio of parameters. This means that if any two parameters out of these three are fixed, one can always adjust the third parameter (for example, the one that can be most easily tuned in the experiment) to maximize the power factor.

Before closing this section, we remark that we have searched for resonant tunneling states in the positive V_B regime as a way to enhance S. However, we have not found any significant increase in S beyond that already discussed. The reason is that, because the potential contains contributions from several Legendre polynomials l, the appearance of a resonant state for one value of l is washed out by the nonresonant conditions in the other channels.

B. Enhancement of the ZT factor

While S and σ are quantities of fundamental interest, for applications it is usually $ZT=S^2\sigma T/\kappa$ that is most important. The electronic relaxation time calculated above leads directly to the electronic thermal conductivity κ_e. Since the total thermal conductivity is the sum of electronic and phonon contributions, $\kappa=\kappa_e+\kappa_{\text{ph}}$, to obtain ZT we also need to calculate κ_{ph}. For this purpose, we adopt a previous method[6,14] that considered the scattering of phonons on nanoinclusions, with the scattering mechanism for short wavelength phonons being the different sound velocities in the host and nanoinclusions. This approach has been shown to give excellent agreement with experiments on nanoscale ErAs inclusions in InGaAs.[6] For $T \gtrsim T_D$ ($T_D=130$ K is the Debye temperature of PbTe) κ_{ph} can be written as[8]

$$\kappa_{\text{ph}} \approx \frac{k_B}{2\pi^2 v_s \hbar^3} \int_0^{k_B T_D} \tau_{\text{ph}} (\hbar\omega)^2 d(\hbar\omega), \tag{42}$$

where v_s is the speed of sound in PbTe, and $\hbar\omega$ is the phonon energy. The phonon relaxation time τ_{ph} is given by

$$\tau_{\text{ph}}^{-1} = \tau_U^{-1} + \tau_D^{-1}, \tag{43}$$

where $\tau_U^{-1}=cT\omega^2$ is the contribution of umklapp scattering[8] and τ_D is due to scattering by nanoinclusions. The constant c was determined from Eq. (42) using the experimental value $\kappa_{\text{ph}}^{\text{bulk}}=2.0$ W/mK for PbTe at $T=300$ K. For τ_D we used the expression derived in Refs. 6 and 14. In the near-geometrical scattering regime ($qR \gtrsim 1$) τ_D reads

$$\tau_D^{-1} = n_i v_s (2\pi R^2)[1 - \sin(2\xi)/\xi + \sin^2(\xi)/\xi^2], \tag{44}$$

where $\xi=qR(v_s/v_s'-1)$, q is the phonon wave vector, and v_s' is the speed of sound inside the inclusion. Numerical tests show that when the difference in the sound velocities is larger than 20% the integrated quantity κ_{ph} weakly depends on this difference and τ_D can be approximated by its geometrical limit value

$$\tau_D^{-1} = n_i v_s (2\pi R^2) = \frac{3}{2}\frac{x}{R} v_s. \tag{45}$$

Note that this phonon scattering regime is opposite to that on point defects where $qR \ll 1$.

Figure 4 shows ZT and its components calculated for $x=5\%$, $R=1.5$ nm, and a doping $n=2.5\times 10^{19}$ cm^{-3}, as a function of temperature. We discuss this doping first because experimental values of ZT and all of its components are readily available for inclusion-free PbTe, and can be compared with our calculations; indeed, the calculated values for ZT, S, σ, and κ [solid lines in Fig. 4(a)–4(d)] are in good agreement with experiment[15] (filled squares) for $T \lesssim 700$ K. (The deviations for $T \gtrsim 700$ K originate in our neglect of the hole contribution to the charge and heat transport). In the presence of nanoinclusions, the individual components of ZT deviate from their bulk PbTe values at all temperatures shown. For $T \gtrsim 400$ K the increase of the Seebeck coefficient is compensated by decrease of the conductivity, and the optimized power factor is close to that of bulk PbTe [see inset in Fig. 4(c)]. At such temperatures the small increase of the ZT factor due to "electron-only" scattering by nanoinclusions [open circles in Fig. 4(a)] is a result of the decrease in κ_e [open circles in Fig. 4(d)]. Comparing the ZT shown by filled and open circles in Fig. 4(a), one can conclude that at a doping $n=2.5\times 10^{19}$ cm^{-3} the enhancement of the optimized ZT is primarily due to decrease of κ_{ph}, at least for $T \gtrsim 400$ K.

To get a more comprehensive understanding of the role of nanoinclusions in enhancing the thermoelectric properties, we show in Fig. 5 the room-temperature ZT factor as a function of the interface potential for two values of the doping. In addition, we plot ZT calculated using the bulk value of the phonon thermal conductivity $\kappa_{\text{ph}}^{\text{bulk}}$ (dotted lines). We first consider the situation of high doping, as depicted in Fig.

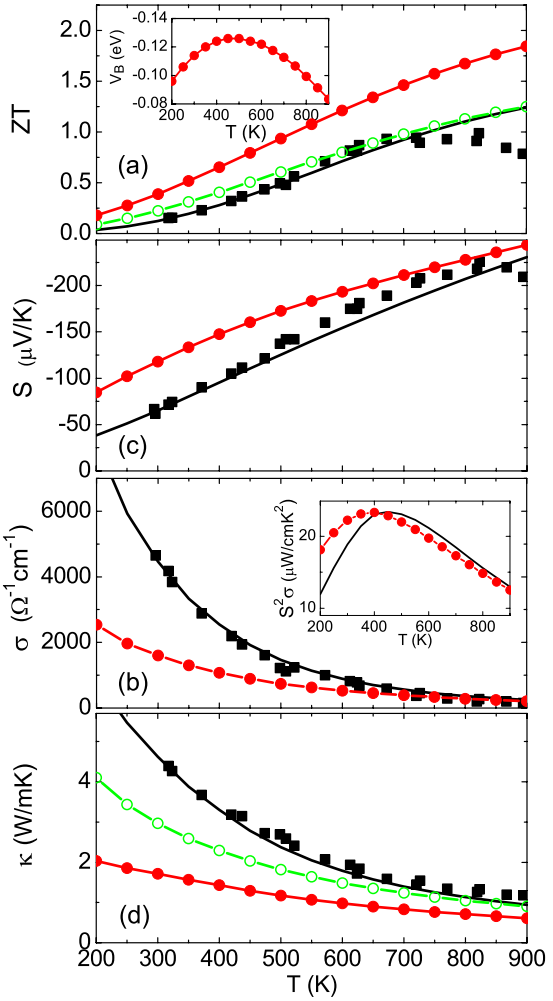

FIG. 4. (Color online) Thermoelectric coefficients as a function of temperature calculated for $n=2.5\times10^{19}$ cm^{-3}, $x=5\%$, and $R=1.5$ nm. (a) The optimized ZT factor, with the optimal values of V_B, is shown in the inset. (b) The Seebeck coefficient. (c) The electrical conductivity. Inset shows optimized (filled circles) and bulk PbTe (solid line) power factor $S^2\sigma$. (d) The thermal conductivity. In all panels, solid circles include electron and phonon scattering on the inclusions; open circles include electron scattering on the inclusions but with bulk PbTe values of κ_{ph}; solid lines and filled squares are the calculated and measured (Ref. 15) values for bulk PbTe.

5(a). In the absence of a spatially-varying potential ($V_B=0$) and without phonon scattering on nanoinclusions, ZT is given by the filled circle. Turning on the phonon scattering gives a modest 25% increase in ZT (the star in the figure). Similarly, one can consider the increase in ZT without phonon scattering on the nanoinclusions (dotted line); in this case, a large increase in ZT of up to 224% is obtained. Thus at this doping, electron scattering can give a much larger increase in ZT. However, the true advantage of nanoinclusions is realized when *both* electron and phonon scattering are included, and the ZT factor can be increased by as much as 430%. This increase is much larger than simply the sum of the individual electronic and phonon contributions.

The origin of this behavior lies in the nonadditive effects of electronic and phonon thermal conductivities, since ZT depends inversely on their sum. For the large doping situation of Fig. 5(a) we have $\kappa_e^{bulk}=4.2$ W/mK, $\kappa_{ph}^{bulk}=2.0$ W/mK, and therefore $\kappa_{ph}^{bulk}<\kappa_e^{bulk}$. In this case, reducing κ_{ph} by itself does not lead to an appreciable gain in ZT. However, when κ_e is also reduced because of scattering and becomes comparable to κ_{ph}, then both work in concert and lead to a large increase in ZT. Thus, one can imagine that electron scattering on the electrostatic potential serves as an amplification mechanism to enhance the impact of the reduction in phonon thermal conductivity. This mechanism works here because at high doping (i) $\kappa_{ph}^{bulk}<\kappa_e^{bulk}$ and (ii) the power factor is maintained or even enhanced in a wide range of interface potentials.

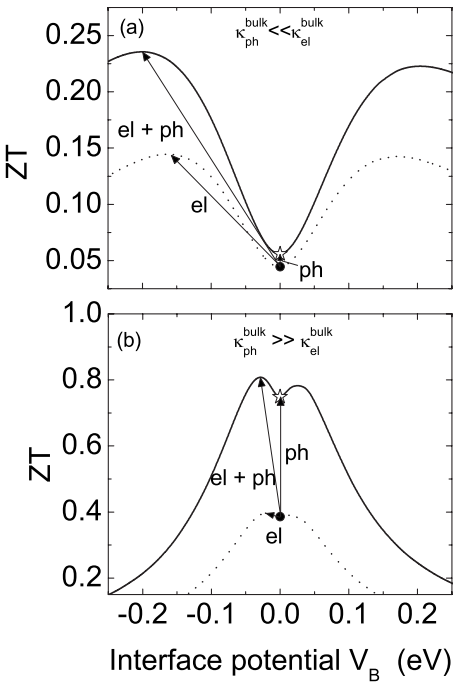

FIG. 5. Calculated ZT factor for PbTe illustrating the relative effects of electronic and phonon scattering on nanoinclusions. In both panels $R=1.5$ nm, $x=5\%$, and $T=300$ K. (a) High doping $n=5\times10^{19}$ cm^{-3}. (b) Low doping $n=5\times10^{18}$ cm^{-3}. Dotted lines are calculated using the bulk phonon thermal conductivity. Filled circles correspond to the bulk PbTe system. Stars include only the phonon scattering on nanoinclusions.

The situation is quite different in the case of low doping, where $\kappa_{ph}^{bulk}\gg\kappa_e^{bulk}$, as illustrated in Fig. 5(b). In this case, the electronic thermal conductivity is already quite low, $\kappa_e^{bulk}=0.6$ W/mK$<\kappa_{ph}^{bulk}=2.0$ W/mK, and the main impact of nanoinclusions is to decrease the phonon thermal conductivity. The maximum increase in ZT is 107%, with 94% coming from phonons alone. In fact, for this low doping, the power factor is always reduced compared to the inclusion-free system——a signature of this effect is the reduction of ZT below that of the inclusion-free system for larger values of V_B.

Figure 6 shows the calculated ZT as a function of temperature for low ($n=5\times10^{18}$ cm^{-3}) and high ($n=5\times10^{19}$ cm^{-3}) doping levels. Included in the figure are the ZT factor calculated with both electron and phonon scattering on nanoinclusions (filled circles), that calculated with electron-

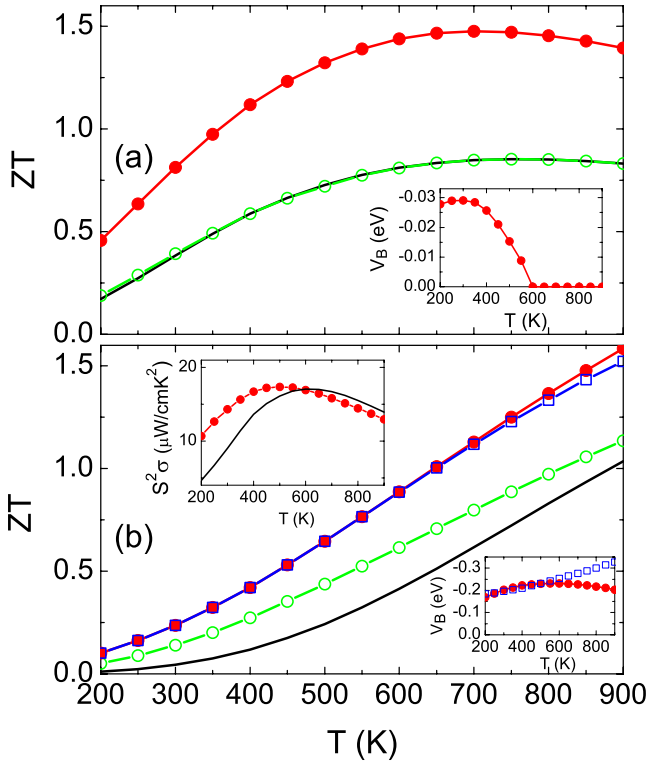

FIG. 6. (Color online) Temperature dependence of the optimized ZT factor for PbTe. (a) low doping $n=5\times10^{18}$ cm^{-3} and (b) high doping $n=5\times10^{19}$ cm^{-3}. In both panels filled circles denote the optimized ZT calculated with both electron and phonon scattering on nanoinclusions, open circles denote ZT calculated with electron scattering on nanoinclusions and with bulk PbTe values of $\kappa_{\rm ph}$, and the solid line is for bulk PbTe. The inset in (a) shows the values of V_B that maximize ZT. In (b) the bottom inset shows the optimal values of V_B that maximize ZT (filled circles) and $V_B^{\rm Pb}$ for Pb nanoinclusions. The top inset shows the calculated power factor.

only scattering on nanoinclusions and with bulk PbTe values of $\kappa_{\rm ph}$ (open circles), and the ZT calculated for inclusion-free bulk PbTe (solid line). The corresponding values of V_B that maximize ZT are shown in the insets by filled circles. The inset in Fig. 6(a) shows that at $n=5\times10^{18}$ cm^{-3}, the optimal V_B is very small $|V_B|<0.03$ eV and even vanishes for $T>600$ K. Thus, the electron contribution to enhancement of optimized ZT is negligible [solid line and line with open circles almost coincide in Fig. 6(a)] and, the enhancement of the optimized ZT is dominated by the reduction in $\kappa_{\rm ph}$ due to phonon scattering on the inclusions. This can be explained by the fact that for bulk PbTe, the Seebeck coefficient increases with decrease of the doping concentration n, and the *relative* enhancement of the Seebeck coefficient from its bulk value due to electron scattering on inclusion is smaller at low doping compared to high doping (see Fig. 2). As a consequence the reduction of σ at low doping overweights the increase of S^2, and the power factor is reduced compared to the inclusion-free system, leading to small or vanishing optimal V_B. From a practical point of view this result means that in order to enhance the ZT factor at low-doping levels one needs to find a metal that gives little or no interfacial potential.

For larger doping the electron contribution to enhancement of ZT becomes important, and the optimized V_B increases. It is seen in Fig. 6(b) that for $n=5\times10^{19}$ cm^{-3}, the electron-only contribution to enhancement of the optimized ZT makes up over 50% of the enhancement at $T\lesssim600$ K, and the optimized V_B is as large as 0.2 eV. Moreover, at large doping, $\kappa_e^{\rm bulk}>\kappa_{\rm ph}^{\rm bulk}$, and the reduction of κ_e due to scattering on inclusions amplifies the effect of the reduced $\kappa_{\rm ph}$. The upper inset in Fig. 6(b) shows that the power factor σS^2 is enhanced only for $T<600$ K. The reduction of the power factor relative to the inclusion-free system at $T>600$ K is due to the fact that at high temperature, the Seebeck coefficient of bulk PbTe is already large [see Fig. 4(b)]; the *relative* increase in S induced by electron scattering on inclusions becomes smaller at increased temperature, so the reduction of σ overweights the increase of S^2. Nevertheless, the electron-only contribution results in enhancement of ZT [open circles in Fig. 6(b)] even at higher temperatures due to reduction of κ_e.

Figure 6(b) shows by open squares the ZT factor for PbTe with Pb inclusions (assuming $V_B^{\rm Pb}-E_F=-0.35$ eV) for parameters $n=5\times10^{19}$ cm^{-3}, $R=1.5$ nm, and $x=5\%$. For this set of parameters the interface potential $V_B^{\rm Pb}$ is close to the optimal one [see inset in Fig. 6(b)] in a wide range of temperatures, so the ZT factor for the system with Pb inclusions is very close to the optimal ZT. The enhancement of ZT due to Pb inclusions is on the order of 400% at room temperature and 50% at $T=900$ K, where it reaches a value as high as 1.5.

V. CONCLUSION

In conclusion, we developed a theory that allows the calculation of the ZT factor and its components for a system of a semiconductor host material with spherical metallic nanoinclusions. The enhancement of the Seebeck coefficient can be explained by a strong energy dependence of electron scattering on the band bending at the interface between metallic inclusions and the semiconductor host. The electronic contribution to enhancement of ZT is important for high doping, while at low doping the enhancement of ZT is dominated by the reduction in the phonon thermal conductivity. The theory can be used to choose the optimal parameters for the metal nanoinclusions (interface potential, inclusion volume fraction or radius) in order to maximize ZT.

ACKNOWLEDGMENTS

We thank Doug Medlin and Peter Sharma for useful discussions. Sandia is a multiprogram laboratory operated by Sandia Corporation, a Lockheed Martin Co., for the United States Department of Energy under Contract No. DE-AC04-94-AL85000.

*sfaleev@gmail.com

[1] T. C. Harman, P. J. Taylor, M. P. Walsh, and B. E. LaForge, Science **297**, 2229 (2002).
[2] R. Venkatasubramanian, E. Siivola, T. Colpitts, and B. O'Quinn, Nature (London) **413**, 597 (2001).
[3] K. F. Hsu, S. Loo, F. Guo, W. Chen, J. S. Dyck, C. Uher, T. Hogan, E. K. Polychroniadis, and M. G. Kanatzidis, Science **303**, 818 (2004).
[4] H. Lin, E. S. Bozin, S. J. L. Billinge, E. Quarez, and M. G. Kanatzidis, Phys. Rev. B **72**, 174113 (2005).
[5] J. P. Heremans, C. M. Thrush, and D. T. Morelli, J. Appl. Phys. **98**, 063703 (2005).
[6] W. Kim, J. Zide, A. Gossard, D. Klenov, S. Stemmer, A. Shakouri, and A. Majumdar, Phys. Rev. Lett. **96**, 045901 (2006).
[7] Yu. I. Ravich, B. A. Efimova, and V. I. Tamarchenko, Phys. Status Solidi B **43**, 11 (1971).
[8] Yu. I. Ravich, B. A. Efimova, and I. A. Smirnov, *Semiconducting Lead Chalcogenides* (Plenum, New York, 1970).
[9] D. M. Zayachuk, Semiconductors **31**, 173 (1997).
[10] L. D. Landau and E. M. Lifshitz, *Quantum Mechanics Nonrelativistic Theory, Course of Theoretical Physics*, 3rd ed. (Nauka, Moscow, 1976), Vol. 3.
[11] H. B. Michaelson, J. Appl. Phys. **48**, 4729 (1977).
[12] W. E. Spicer and G. T. Lapeyre, Phys. Rev. **139**, A565 (1965).
[13] Yu. I. Ravich, B. A. Efimova, and V. I. Tamarchenko, Phys. Status Solidi B **43**, 453 (1971); B. A. Efimova, L. A. Kolomoets, Yu. I. Ravich, and T. S. Stavitskaya, Sov. Phys. Semicond. **4**, 1653 (1971).
[14] W. Kim and A. Majumdar, J. Appl. Phys. **99**, 084306 (2006).
[15] B. A. Efimova, L. A. Kolomoets, Yu. I. Ravich, and T. S. Stavitskaya, Sov. Phys. Semicond. **4**, 1653 (1971).